Computational Materials Science 212 (2022) 111549

Contents lists available at ScienceDirect

Computational Materials Science

journal homepage: www.elsevier.com/locate/commatsci

Full Length Article

A molecular dynamics simulation study on the role of graphene in enhancing the arc erosion resistance of Cu metal matrix

Ruoyu Xu [a], Mingyu Zhou [a,b], Xin Wang [c], Shanika Yasantha Matharage [c], Jiu Dun Yan [d], Andrew Connolly [e], Yi Luo [a], Yi Ding [b,f], Zhongdong Wang [c,*]

[a] Global Energy Interconnection Research Institute Europe GmbH, Kantstr. 162, 10623 Berlin, Germany
[b] State Key Laboratory of Advanced Power Transmission Technology (Global Energy Interconnection Research Institute Co, Ltd.), 18 Binhe Ave, 102209 Beijing, China
[c] Centre for Smart Grid, Department of Engineering, University of Exeter, EX4 4PY, UK
[d] Department of Electrical Engineering and Electronics, University of Liverpool, Liverpool L69 3GJ, UK
[e] Department of Materials, University of Manchester, Manchester M13 9PL, UK
[f] State Grid Zhejiang Electric Power Co., Ltd., Hangzhou 310013, China

ARTICLE INFO

Keywords:
Molecular dynamics simulation
Metal matrix composites
Circuit breaker
Arc erosion
Ion bombardment
Graphene reinforcement mechanisms

ABSTRACT

Molecular dynamics simulation has been applied to study the mechanisms through which graphene protects Cu from arc erosion in Cu-W arcing contacts. The impact of arc erosion has been simplified as positive ion bombardments on a cathode surface. Sulphur ions were used as incident ions while the number of ions, incident energy, and incident area varied during the simulations. Cu covered by a graphene layer had fewer vacancies and sputtered atoms than in the pure Cu system. Results show that the graphene layer can dissipate the energy transferred from incident ions by a shock wave, and also prevent recoiled Cu atoms from penetrating the graphene layer resulting in better arc erosion performances than in the pure Cu system. For both models, the sputtering yield gradually decreases and maintains a very low value as the number of incident ions increases. Similar to the experimental results, the residual erosion crater on the Cu surface covered by graphene was shallower than that without a graphene layer.

1. Introduction

In industrial plasma systems, such as high voltage gas blast circuit breakers (HVCB) [1,2] and arc plasma generators [3,4], one or more electric arcs (plasma sustained by an electric current) burn between two solid conductors. These conductors are named electrodes or electrical contacts. One of them acts as a cathode and the other one as an anode. The arc can attain a temperature as high as 20,000 K due to strong Ohmic heating (10^{12} W/m^3). Interaction between the arc and the electrical contacts can be in the form of collisions (such as ion bombardment onto the cathode surface) or energy transfer (such as radiation), leading to consumption of the solid contact material. Arc contact erosion is a major concern in the design of circuit breakers as it is one of the key factors that determine the service life of such devices designed to interrupt high fault currents up to 60 kA [5,6].

Copper-tungsten metal matrix composites (Cu-W MMCs) are the most widely used electrical contact materials in HVCBs. Cu-W MMCs consist of a W matrix with Cu being melted into the W skeleton, taking advantage of the excellent electrical and thermal conductivity properties of Cu, as well as the good mechanical properties and outstanding arc resistance performance of W [7–14]. With continuous switching cycles, Cu on the surface will be lost due to arc erosion, resulting in damages to the structure of the arcing contacts. The degradation of arcing contacts not only reduces its lifetime but also reduces the reliability of the circuit breaker. Therefore, the development of novel contact materials with improved erosion-resisting performance remains a strong need in the switchgear industry.

In general, adding reinforcements is an approach to altering the properties of MMCs. Graphene is a two-dimensional (2D) sheet consisting of covalently bonded sp^2-hybridised carbon atoms with exceptional electrical, mechanical and thermal properties [15–18]. Graphene is considered an attractive reinforcement to enhance the mechanical properties (such as hardness and strength) of MMCs, including Gr-Cu [19–25], Gr-Cu-W [26], Gr-Fe [27], and Gr-Al [28–30]. Recent studies have shown that graphene can improve the arc erosion resistance of MMCs. Dong et al. [31,32] fabricated the Gr-W70Cu30 MMCs (i.e. 70% of W and 30% of Cu in mass percentage composites doped with 0.5 wt% graphene). The results of vacuum electrical breakdown tests under 10

* Corresponding author.

https://doi.org/10.1016/j.commatsci.2022.111549
Received 5 April 2022; Received in revised form 19 May 2022; Accepted 22 May 2022
Available online 11 June 2022

kV showed that the addition of graphene can increase the breakdown strength by ~45.5%, while resulting in a drastic decrease in the weight loss. Due to the reduction in the sputter of molten Cu, cathode craters in Gr-W70Cu30 MMCs were smaller in diameter and shallower than W70Cu30 MMCs. It has been proposed that the low work function and the high melting point of graphene could be the reason for the improvement in arc erosion resistance.

The location of arc generation is related to the work function of contact materials in such a way that the arc tends to be formed at the phase with the lowest work function [9,13,31]. Hence, the arc prefers to occur on the Cu rich zones in Cu-W MMCs as the work function of Cu ($\Phi_{Cu(1\,1\,1)} = 4.95$ eV [33]) is lower than that of W ($\Phi_{W(1\,1\,0)} = 5.26$ eV [34]), resulting in the melting, evaporation and sputtering of a large amount of Cu. However, the work function of graphene ($\Phi_{graphene} = 4.48$ eV [35]) is lower than that of Cu. Therefore, in graphene reinforced Cu-W MMCs, the arc tends to be formed on graphene instead of the Cu region. Besides, graphene has a much higher melting point than Cu (Graphene: $T_m \approx 4900$ K [36], Cu: $T_m = 1358$ K [37]), and hence it can absorb more arc energy than Cu before the meltdown process [31]. As a result, the addition of graphene decreases the impact of the arc on Cu regions, resulting in a decrease in the Cu mass loss.

It is noted that the above explanation is based on the properties of materials, such as work function and melting point. So far, the role of graphene in MMCs during arc erosion has not been investigated from a molecular or atomic level by experiments or simulations. Therefore, in the present work, molecular dynamics (MD) simulation is employed to investigate the mechanism by which graphene protects Cu from arc erosion. The pure Cu and Gr-Cu systems were selected as simulation objects as the loss of Cu is the leading cause of electrical contacts failure in Cu-W MMCs. The effects of ion bombardment on Cu and Gr-Cu systems were investigated in relation to the following parameters: incident ion kinetic energy, number of incident ions, and size of bombardment area.

2. Simplifications and definition of the problem

2.1. Simplifications of the impacts of arc erosion on cathode materials

Arc erosion of electrical contact is a complex phenomenon. In a breaking operation, when the arcing contacts begin to separate, a conducting bridge made of molten metal is first formed between the surfaces of the two contacts due to the concentrated heat produced by the current which passes through the electrically connected points. The bridge becomes unstable and eventually ruptures as the contacts continue to move apart, which leads to the release of metal vapour into the contact gap space. As the contact moves, an arc with a cathode region supplying electrons to carry the current between the contacts is formed [38]. The metal ions move toward the cathode surface under the applied electric field and collide with the cathode. As the contact gap increases and the percentage of metal vapour in the arc declines, the ambient gas will enter the arc. Thus, the nature of the arc converts to a gaseous arc. The ambient gas becomes the dominant ionised plasma in the arc [38,39]. The gas ions gain energy when they pass through the space charge sheath [40] near the cathode surface and then bombard the cathode surface, resulting in the mass loss of the cathode materials. As the gaseous arc continues, a cathode crater is formed. It is noted that when approaching the cathode surface, the ions are neutralised by the electrons emitted from the cathode surface, but the process is commonly known as ion bombardment in the switching arc community. Hence, the term “ion bombardment” is retained in the paper to provide a bridge between the present work and the arcing process in circuit breakers. However, one should know that it is the atoms that are bombarded onto the cathode surface, not the ions.

Due to the complexity of arc contact erosion and a lack of essential knowledge at the microscopic level, most of the existing models available for composite materials are either empirical (for high current) [41] or based on consideration of energy balance [42,43]. The present work is not intended for a comprehensive model for the whole erosion process, nor does it consider all practical conditions encountered in circuit breaker operations. Instead, we focus on an important aspect of the particle interaction between the arc and the contact surface, i.e. the bombardment of positive ions on the cathode surface. These energetic ions collide with the cathode surface and provide a dominant majority of the energy flux [44], resulting in the erosion process. It is expected that knowledge on the interaction of positive ions with the cathode will form one of the supporting pillars to develop a science-based comprehensive model to predict the arc erosion process of electrical contacts. Although simplifications are made, the conditions used in the present work are representative or meaningful with respect to problems in practical applications.

2.2. Incident energy of ions in a circuit breaker arc

The present simulation work focuses on SF_6 filled circuit breakers due to their predominance in HVCB. Out of different ions (metal, sulphur, positive fluorine) involved in the bombardment process, the sulphur ion was selected as the incident ion to study the protective mechanisms of graphene. The kinetic energy range of sulphur ions was estimated using literature on ion incident energy which is a combination of thermal energy from the arc, kinetic energy from the voltage drop at the cathode region and recombination energy. The average thermal energy (E_{th}) of the ions in the arc ranges from around 0.85 eV for low-current arcs to around 2.5 eV for high-current arcs due to the high temperature of arc column [39]. Furthermore, ions will be accelerated by a voltage drop (V_c) (usually between 10 and 20 V) at the cathode region, gaining kinetic energy (E_V), given by:

$$\boldsymbol{E_V = ZeV_c} \tag{2-1}$$

where Z is the number of charges of the ion. Z could be 1 or 2 for sulphur ions because both S^+ and S^{2+} exist in the arc plasma [45,46]. e is the elementary charge ($\approx 1.602 \times 10^{-19}$C). Therefore, E_V ranges from 10 eV to 40 eV.

Finally, ions will recombine with emitted electrons before arriving at the cathode surface, during which the ions obtain ionisation energy E_i, given by

$$\boldsymbol{E_i = ZV_i} \tag{2-2}$$

where Z is the number of charges of the ion and V_i is ionisation potential, which is 10.99 eV for sulphur atom [47]. Hence, E_i ranges from around 11 eV to 22 eV.

Therefore, the total energy of an incident ion $E_{total} = E_{th} + E_V + E_i$ is approximately between 22 eV and 65 eV. Considering the energy fluctuations of the ions in the arc, such as impacted by collisions with other ions or neutral atoms, the energy of some ions will be less than this range, and the energy of some ions will be beyond this range. Therefore, the incident ion energy values of 20 eV, 50 eV and 100 eV were selected for the simulations.

3. Simulation methodology

Molecular dynamics simulations were performed using the Large-scale Atomic/Molecular Massively Parallel Simulator (LAMMPS) [48]. The adaptive intermolecular reactive empirical bond order (AIREBO) potential [49] was used to describe the interactions between C atoms in graphene. The interaction between Cu atoms was described by the embedded atom method (EAM) potential, splined to the Ziegler Biersacke Littmark (ZBL) repulsive potential [50], which has been used for the radiation simulation of the Cu-graphene system [51]. The van der Waals force between Cu and C atom pair was described by the 12–6 Lennard-Jones (L-J) potential, given by Eq. (3-1), where E is the total energy between a pair of Cu atom and C atom; r is the distance between

Cu atom and C atom; r_c is the cutoff distance; ε is the well depth and δ is an equilibrium distance. In the present work, ε = 0.019996 eV, δ = 3.225 Å [20,51,52] and $r_c = 5\,\delta$. The interactions between the incident S atom with C, Cu, and other S atoms were calculated with the ZBL repulsive potential [53].

$$\boldsymbol{E} = 4\boldsymbol{\varepsilon}\left[\left(\frac{\boldsymbol{\delta}}{\boldsymbol{r}}\right)^{12} - \left(\frac{\boldsymbol{\delta}}{\boldsymbol{r}}\right)^{6}\right], \boldsymbol{r} < \boldsymbol{r_c} \tag{3-1}$$

The schematic diagrams of the pure Cu model and the Cu model covered with a single layer of Gr used for ion bombardment simulations are shown in Fig. 1. The crystallographic orientations of Cu are x [−1 1 0], y [−1 −1 2], and z [1 1 1]. The fixed boundary condition is used along the z direction, while the periodical boundary condition is applied in the x and y directions. Furthermore, the location of the two bottom layers in Cu the substrate is fixed.

The energy of the models was first minimised and then the models were fully relaxed at 300 K prior to the bombardment simulation. Under typical operating conditions, the temperature of the arc contacts would reach the boiling point of contact materials. However, the initial temperature of the model was set at 300 K to avoid the evaporation of Cu atoms due to the initial high temperature and to study the impact of only the ion bombardment process. During ions bombardment, three atom layers at all four vertical faces were forced to maintain 300 K through the Berendsen temperature control method to prevent the waves caused by the bombardment from returning through the periodic boundary. As described in Section 2, ions are neutralised before bombarding the cathode surface, so the charges of ions were not considered, and neutral sulphur atoms instead of sulphur ions were used for bombardment in the simulation. However, we refer to the incident particle as an "ion", as ion bombardment is a common term in the switching arc research community.

The simulations were divided into single ion bombardment and multiple ions bombardment. The purpose of single ion bombardment is to observe the behaviour of the graphene layer, while multiple ions bombardment aims to simulate arc erosion. In single ion bombardment, the incident ion was placed at the centre above 5 nm from the model surface, and incident energy ranging from 20 eV to 1000 eV was selected to observe the behaviour of the graphene layer at high incident energy values. Each simulation was repeated 20 times to identify the statistical deviations in the result.

In multiple ions bombardment simulation, the model surface was continuously bombarded with ions appearing from random sites within a circular region above 5 nm from the model surface. Two different exposure areas with a diameter of 2 nm and 4 nm were simulated to study the influence of the size of the arc root. The number of incident ions (incident dose) was varied from 10 to 300, and the time interval between atoms was set as 0.1 ps. The energy of each ion was set to 20 eV, 50 eV or 100 eV in different simulations. An NVE ensemble was used during the bombardment process, with a variable timestep depending on the incident energy. After the bombardment of 300 ions, the simulation was continued for 20 ps to facilitate the natural energy transfer process before cooling down to 300 K within 100 ps and finally conducted a further relaxation for 50 ps at 300 K to stabilise the system. The peak number of vacancy defects, the total number of sputtered Cu atoms and the residual surface morphology at the end of the simulation were used to indicate the damages to Cu during the ion bombardment process.

4. Results and discussion

4.1. Single ion bombardment simulations

This section presents the results of the single sulphur ion bombardment simulation conducted on pure Cu and Gr-Cu systems. Through analysing the number of vacancies and sputtering yield of Cu atoms, it explores the mechanisms through which graphene protects Cu from arc erosion.

4.1.1. Peak number of vacancies

During the bombardment process, collisions transfer energy from the incident ion to the target atoms. The atoms gaining energy will move from lattice sites and collide with other atoms, resulting in vacancies and interstitial lattice defects, which affect the mechanical, electrical and thermal properties of crystal materials. Hence, the number of vacancies or interstitials is often used to quantitatively evaluate the impact of bombardment or radiation on crystalline materials [51,54]. Fig. 2 shows the average peak vacancy number in the bulk Cu region obtained from 20 independent simulations plotted against the respective incident energy values. The peak number of vacancies of the pure Cu system is higher than that of the Gr-Cu system. Moreover, the difference in peak vacancy number between pure Cu and Gr-Cu increases with incident energies.

For the Gr-Cu system, the ion impact results in an elastic bulging of the graphene and underlying Cu. The graphene layer absorbs some of the collision energy and dissipates it in the form of a shock wave that propagates along the graphene layer. This reduces the energy transmitted to the underlying Cu by collision, which results in a less number of vacancies being formed in the bulk Cu region compared to the number of vacancies in the pure Cu system.

4.1.2. Sputtering yield

Sputtering yield Y, defined as the average number of atoms removed per incident ion, is used to quantify the sputtering process. The theoretical value of the sputtering yield can be calculated using Eq. (4-1) [55].

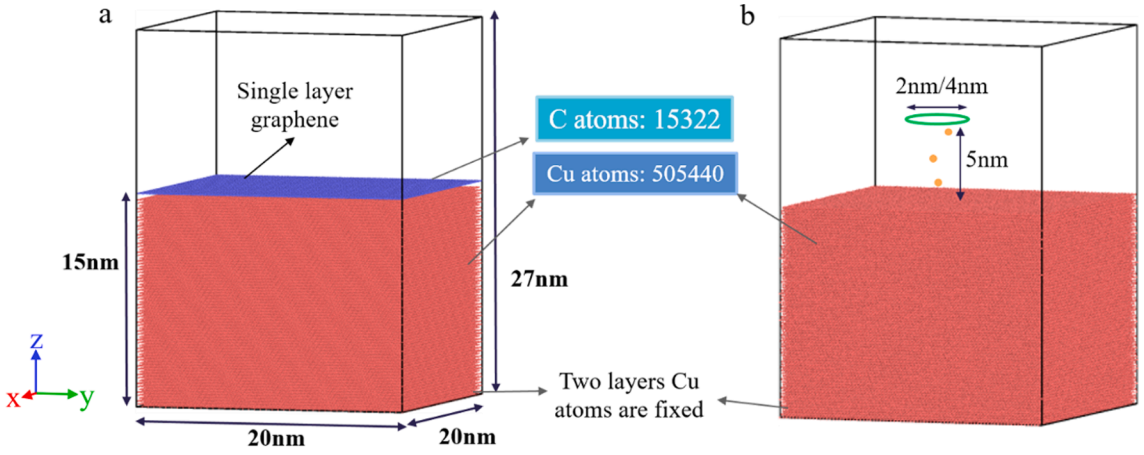

Fig. 1. The schematic diagram of the models: (a) graphene-Cu model; (b) pure Cu model.

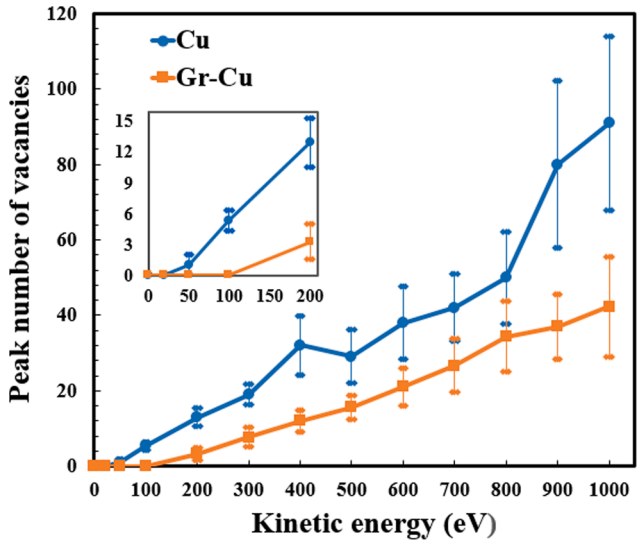

Fig. 2. Peak number of vacancies in pure Cu and the Cu region of Gr-Cu systems at different incident energy values. The inset shows a zoomed in version for the incident energy between 0 and 200 eV.

$$Y = 0.3\frac{M_1 M_2}{(M_1 + M_2)^2}\alpha\frac{E_{in}}{U_0}(\quad \text{4-1)}$$

where M_1 and M_2 are the mass of the incident ion (S) and target atom (Cu), respectively; E_{in} is the incident energy; α is a correction factor depending on the M_2/M_1. For S and Cu, α is 0.4 [56]. U_0 denotes the surface bonding energy, and it is 4.38 eV [57] for Cu.

The sputtering yield values calculated from Eq. (4-1) and the simulations are presented in Fig. 3. It can be seen that the simulation results of the pure Cu system are comparable to the calculated values, which validates the simulation strategy. The average sputtering yield of Cu at 100 eV was 0.05, and it continued to increase with the increase in incident energy. Conversely, for the Gr-Cu system, a sulphur ion with energy up to 1000 eV failed to sputter any Cu atoms for collisions. Simulation indicated that an ion requires at least 100 eV to penetrate the graphene layer to bombard the underlying Cu bulk. To further study the energy threshold (E_t) for a single sulphur ion to penetrate the graphene

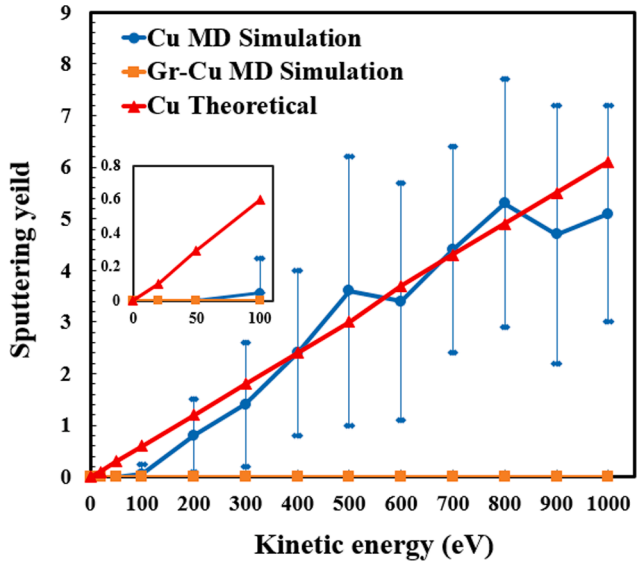

Fig. 3. Sputtering yield of Cu for pure Cu and Gr-Cu systems for single ion bombardment. The inset shows a zoomed in version for the incident energy between 0 and 100 eV.

layer, additional simulations were conducted with an incident energy value ranging between 80 eV and 100 eV with increments of 5 eV. Based on 20 repetitive simulations at each energy level, E_t was found to be ~85 eV. (In the case of 85 eV, none of the atoms penetrated graphene, while for the case of 90 eV, 4 out of 20 simulations indicated a penetration.) Even though sulphur penetrates graphene at incident energy values above the threshold, most of the collision energy is still effectively dissipated by the graphene. Therefore, the Cu atoms beneath the collision site that recoil from deformation as a result of the collision do not have sufficient energy to penetrate the graphene layer. Furthermore, the vacancy (damaged area) in graphene caused by an incident ion is too small for the recoiled Cu atoms to escape. Hence, graphene can effectively protect Cu from sputtering caused by single ion bombardment even at an incident energy of 1000 eV.

4.2. Multiple ions bombardment simulation

Continuous ion bombardment of the model surface with multiple sulphur ions was simulated to study the arc erosion effect. The study was conducted with an incident area diameter of 2 nm, and the incident dose was varied from 10 to 300. The mechanism of arc erosion and the protective effect of graphene on Cu were explored by analysing the number of vacancies, the number of sputtered Cu atoms, features of the erosion crater and other surface morphologies.

4.2.1. Peak number of vacancies

Fig. 4 shows the peak number of vacancies in the Cu region for both pure Cu and Gr-Cu systems bombarded by sulphur ions with different incident doses. Under the same bombardment conditions, the number of vacancies in the Cu region of Gr-Cu is always lower than that in pure Cu, indicating graphene's ability to reduce the damage to bulk Cu during the ion bombardment. The protective properties of a graphene layer are observed to be highly pronounced, with the Gr-Cu system when bombarded at an ion energy of 50 eV outperforming a pure Cu system bombarded at 20 eV. In pure Cu systems, the number of vacancies first increases significantly as the number of incident ions increases before plateauing at about 250 incident ions.

In the Gr-Cu system, when the incident energy was 20 eV, even 300 sulphur ions could not create any vacancy in the Cu region of the Gr-Cu system. This was due to the inability of sulphur ions to penetrate through the graphene layer and bombard the Cu bulk. In addition, the energy transferred to graphene through the bombardment was not enough to create a vacancy in Cu bulk through the collision between the graphene layer and the top layers of Cu atoms. During the bombardment with an incident energy of 50 eV, it required more than 50 incident ions to break

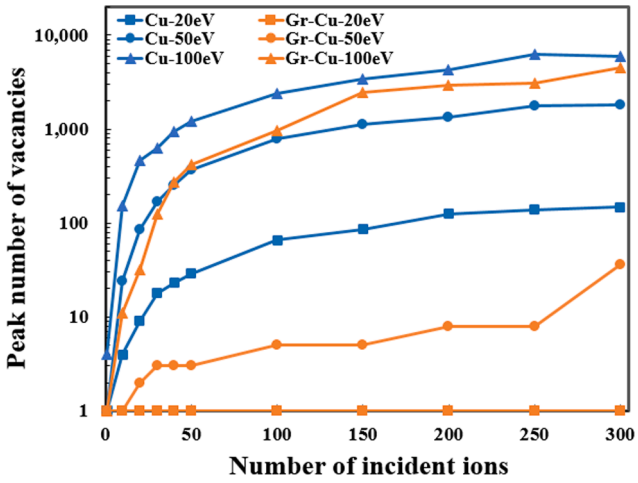

Fig. 4. Peak number of vacancies in the Cu region for pure Cu and Gr-Cu for ion bombardment with multiple ions.

the C—C bond and penetrate through the graphene layer. The structure of graphene after bombarding by 50 incident ions is shown in Fig. 5(a). As the number of incident ions increases to around 100, some of the C—C bonds in graphene become unstable and form vacancies in graphene, as shown in Fig. 5(b). With a further increase in the number of incident ions, adjacent vacancies are combined together to form larger "nanopores" in the graphene layer, surrounded by chains of the remaining neighbouring carbon atoms. As the number of incident ions increases, the size of these nanopores increases, as shown in Fig. 5(c) and (d) due to ion collisions occurring in close proximity to each other on the graphene layer. These nanopores in the graphene layer expose the underlying Cu bulk, and the Cu is then bombarded by the subsequent incident ions resulting in a significant increase in the peak number of vacancy defects, as shown in Fig. 4. Bombardment at higher energy levels such as the 100 eV will easily break C—C bonds, and hence the nanopores will be formed earlier and ultimately grow to a larger lateral size. Therefore at 100 eV incident energy level, the number of vacancies in Cu bulk shows rapid growth. At high incident dose values, the peak number of vacancies in the Cu bulk of the Gr-Cu system is similar to that in the pure Cu.

4.2.2. *Number of sputtered Cu atoms*

The number of sputtered Cu atoms from pure Cu and Gr-Cu systems at 50 eV and 100 eV are shown in Fig. 6. Results for 20 eV are not shown as the energy was not enough to cause sputtered Cu atoms.

It can be seen that the number of sputtered Cu atoms in the pure Cu system increases rapidly with the number of incident ions during the first 50 incident ion bombardment and later tends to level-off at the high number of incident ions. The sputtering yield can be described by the slope of a curve in Fig. 6, which means that the sputtering yield decreases with increased incident ions. A similar phenomenon was observed when Ru single crystal was bombarded with Ar^+ ions [58]. The sputtering yield of Ru atoms in the experiment decreased with the increase in incident dose and reached a steady state at high incident dose values. Moreover, the experimental data revealed that the sputtering yield of the intact surface was twice that of the damaged surface, indicating that the sputtering yield is related to the surface structure. It seems that the surface vacancies created by the initially bombarded atoms later hinder the atom sputtering process. This agrees with MD simulation results [59], which demonstrated that changes in the surface structure on the atomic scale cause a decrease in the sputtering yield.

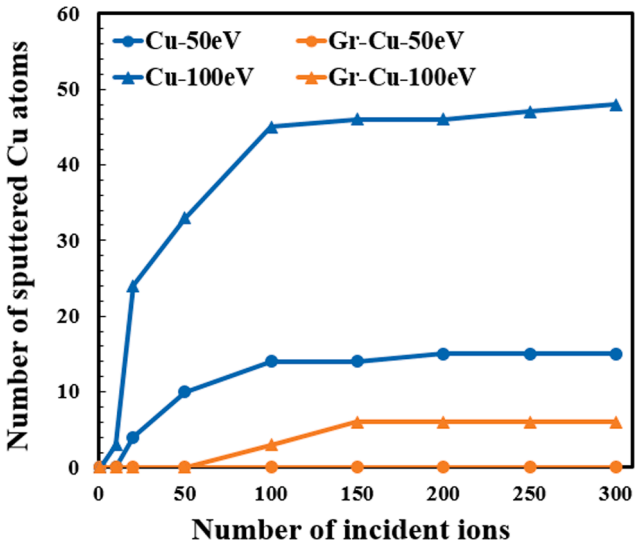

Fig. 6. Number of sputtered Cu atoms during the ion bombardment with multiple ions.

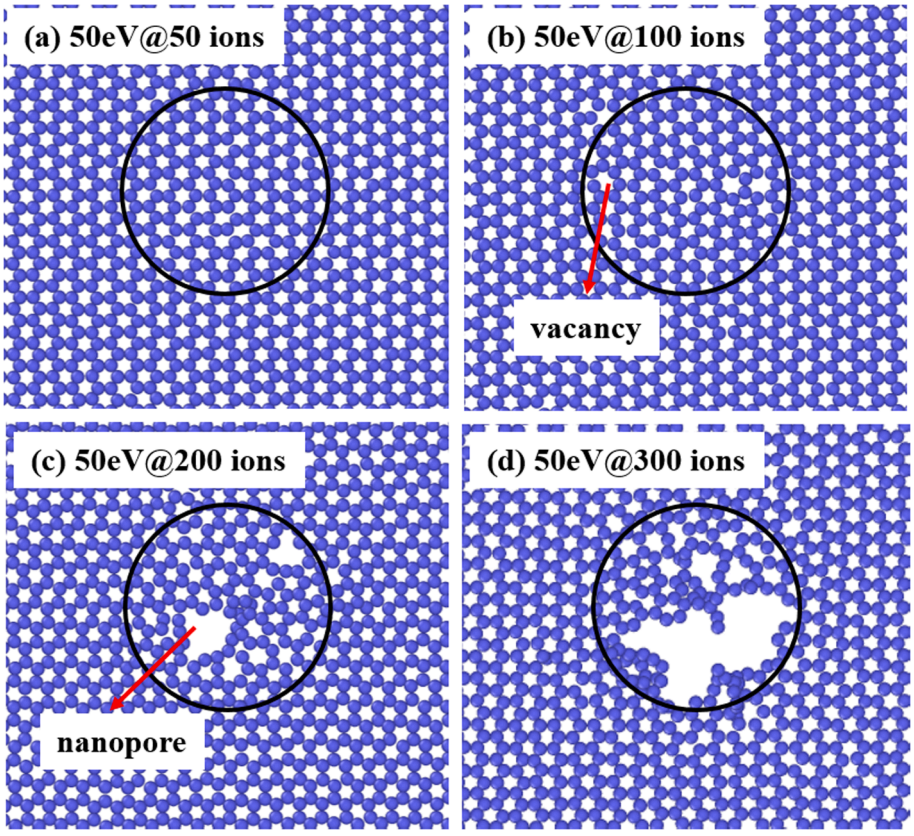

Fig. 5. Structure of graphene when bombarded with different doses of sulphur ions with 50 eV incident energy. Black circle shows the window of ion bombardment. Cu bulk and sulphur ions are not shown.

In the present work, when the initial incident ions impact the Cu surface, the Cu atoms rapidly gain energy and collide with surrounding atoms to generate secondary recoils. Some recoiled atoms can overcome the surface binding energy to become sputtered atoms. In general, secondary recoils contribute to most sputtered atoms [60]. The surface is continuously damaged during the process resulting in an erosion crater. Fig. 7 shows the development of the erosion crater during the bombardment.

Fig. 7(a) shows that a shallow crater is formed after the first 50 ions bombardment. Small crater depths occurred with low incident dose values further support the sputtering process resulting in the initial rapid increase in the number of sputtered atoms. With the increase in the incident dose, a deeper erosion crater is formed as shown in Fig. 7(b). However, as the crater gets deeper, sputtering of atoms from the deep positions becomes difficult due to the lack of energy in the bombarded atoms to overcome the binding energy of their current position. Also, most of the sputtered atoms will frequently collide with the molten walls of the crater and recombine. It is noted that during the bombardment process, the point defects in the Cu constantly recombine to recover the initial structure. As shown in Fig. 7(d)–(f), the erosion crate depth no longer changes significantly as the recovery rate is balanced with the damages caused by ion bombardment. This explains the plateauing behaviour noted with the peak number of vacancies shown in Fig. 4.

The ion bombardment process also impacts the temperature of the model. Fig. 8 shows the temperature distribution of atoms at the surface of the pure Cu system after the ion bombardment with an ion dose of 100 ions at an incident energy of 100 eV. It can be seen that the temperature of many Cu atoms in the crater has reached the boiling point of Cu. Therefore, evaporation will play a major role in the subsequent sputtering process of Cu atoms.

The multiple ion bombardment process in the Gr-Cu system was explained in Fig. 5, when analysing the peak vacancy numbers in the Gr-Cu system. Simulation with 50 eV incident energy indicated that an ion dose of 100 ions cannot cause apparent damage to the graphene structure. The energy of the incident ions is partially transferred to the graphene layer and dissipated mainly in the form of a shock wave. Only a small portion of the energy is transferred to the Cu bulk. When the ion dose is 200, some carbon atoms in graphene are sputtered by the first set of bombarded ions resulting in nanopores within the graphene layer. This allows some of the subsequent incident ions to bombard the exposed Cu surface. Nonetheless, it is still difficult for Cu atoms to leave from nanopores due to the low probability of direct bombardment and small nanopore size.

When the incident energy is 100 eV, the graphene structure is destroyed earlier to form nanopores. Most of the C—C bonds in the

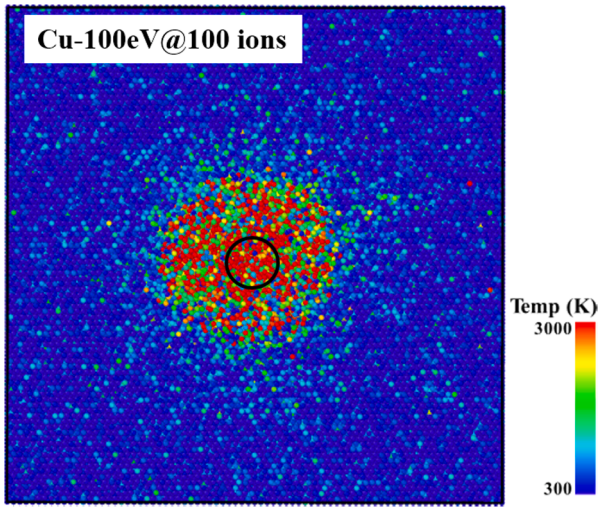

Fig. 8. Surface temperature distribution in the pure Cu after the ion bombardment with an ion dose of 100 ions at an incident energy level of 100 eV. Colour represents the temperature. When the temperature exceeds 3000 K, the colour is the same as 3000 K. The black circle shows the window of the bombardment. (For interpretation of the references to colour in this figure legend, the reader is referred to the web version of this article.)

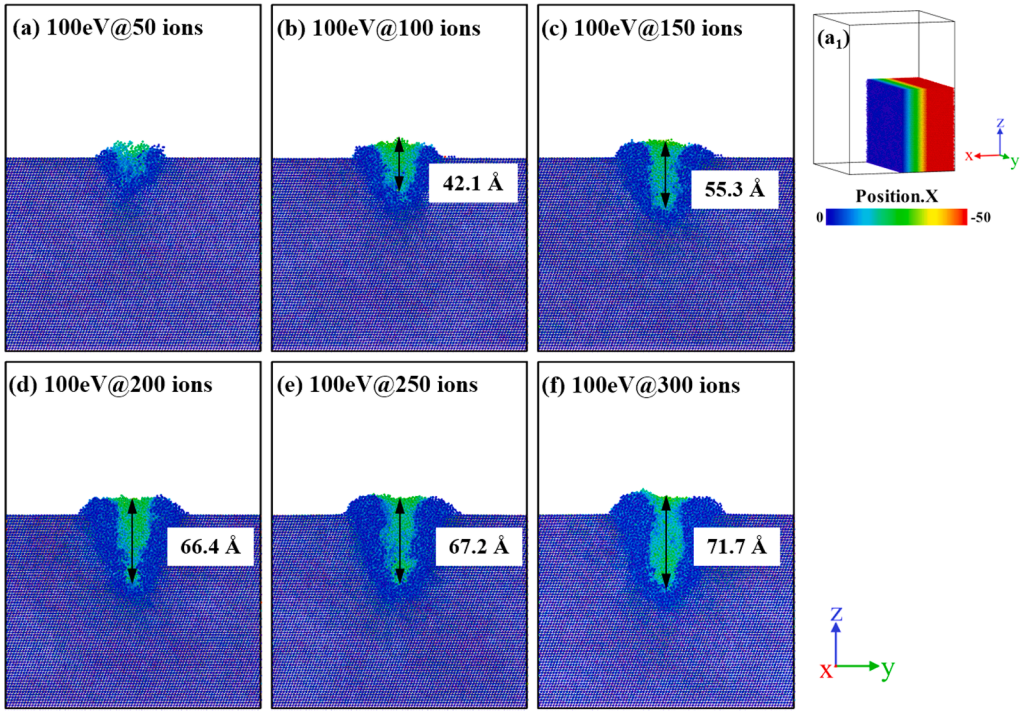

Fig. 7. Cross section of pure Cu after bombardment process with different ion doses at an incident energy of 100 eV. a_1 is from the side view, and the rest are from the view of the x-axis. Colour represents the position of an atom along the x-axis. Atoms floating above the model surface are not displayed. (For interpretation of the references to colour in this figure legend, the reader is referred to the web version of this article.)

incident area are broken by the first 50 atoms, and the size of the nanopore becomes similar to the incident area. Hence, the following incident ions are directly bombarded onto the Cu bulk resulting in an increase in the number of sputtered Cu atoms. Similar to the pure Cu system, the sputtering yield decreases with the increase in the depth of the erosion crater. In addition, a large number of recoiled Cu atoms collide with graphene, resulting in a temperature rise and bulging of graphene. However, the excellent mechanical strength and the high melting point of graphene prevent the recoiled Cu atoms from penetrating the graphene layer. Hence, the sputtered Cu atoms have to pass through the nanopore, which significantly limits the sputtering yield. Therefore, the number of sputtered Cu atoms in the Gr-Cu system is much lower than that of pure Cu.

4.2.3. Morphologies of erosion craters

Surface morphology, which can be evaluated from various imaging technologies, is typically used to study the impact of arc erosion on the contact surface [31,61]. A similar evaluation was conducted with both pure Cu and Gr-Cu systems by comparing the sizes of the erosion craters and the surface morphologies. Fig. 9(a)–(d) shows the snapshots of models at the end of the multiple ion bombardment process with an ion dose of 300 ions at different incident energy values, and Fig. 9(e)–(h) shows the cross section of the respective erosion craters. It can be seen that the model surfaces have bulged due to the ion bombardment. Compared with the pure Cu system, the height of the bulge is lower in the Gr-Cu system as graphene restricts the upward movement of the Cu atoms. When the incident ion energy is 50 eV, almost no erosion crater is formed in the Gr-Cu system, while there was a crater formed with a depth of around 41.6 Å in the pure Cu system. At high incident energy of 100 eV, a noticeable erosion crater is created in the Gr-Cu system, but the depth is much smaller than that in the Cu system. It indicates that the presence of graphene can effectively reduce the damages to Cu, especially when the incident energy is below the threshold energy of penetrating a graphene layer E_t (~85 eV).

At the end of the bombardment process, the simulation model gradually recovers, decreasing the temperature and the number of vacancies in the system. Furthermore, the volume of the erosion crater decreases as the model surface gradually returns to its initial flat state. The morphologies of the model surfaces when the systems were cooled to 300 K are shown in Fig. 10. It can be seen that the residual erosion craters after the cooling process are shallower than those obtained right after the bombardment process, as in Fig. 9. When the incident energy is set at 50 eV, there is almost no residual pit formed on the Cu surface in the Gr-Cu system while a considerably large residual pit was available in the pure Cu system. This is consistent with the experimental results by Dong et al.[31] in which arcing resulted in the surface of graphene-enhanced Cu-W MMCs to be more even than that of traditional Cu-W MMCs. When the incident energy is increased to 100 eV, the graphene coating makes Cu atoms spread on the surface, resulting in a smoother but larger residual erosion crater on the Cu surface in the Gr-Cu system than that of the pure Cu surface. However, a bubble is formed in the pure Cu system since some sulphur ions remain inside during cooling, as shown in the illustration of Fig. 10(c). As the crater formed during the bombardment process is narrow and deep, the top half of the crater is closed first during the recovery phase. Therefore, some sulphur ions are trapped in the Cu, forming a bubble, which will affect the properties of the materials.

4.3. Influence of the size of the incident area

The effect of arc root size was studied through multiple ion bombardment simulations conducted with incident region diameter values of 2 nm and 4 nm. Fig. 11 shows the number of sputtered Cu atoms in pure Cu and Gr-Cu systems obtained during the simulations conducted with an ion dose of 300 ions at 50 eV and 100 eV incident energy levels. Incident energy of 20 eV was not considered as earlier simulations indicated that 20 eV is not sufficient enough to sputter atoms in both the pure Cu system and the Gr-Cu system.

Simulations with both 50 eV and 100 eV incident energy values show that an increase in the incident area diameter from 2 nm to 4 nm results in a significant increase in the number of sputtered Cu atoms. Even though an increase in the incident area diameter results in a reduction in the energy per unit area, the erosion crater becomes shallower with a larger diameter, as shown in Fig. 12, which facilitates the sputtering process. Based on the calculation in Section 2, it was noted that the energy of most ions in the circuit breaker arc is about 50 eV. According

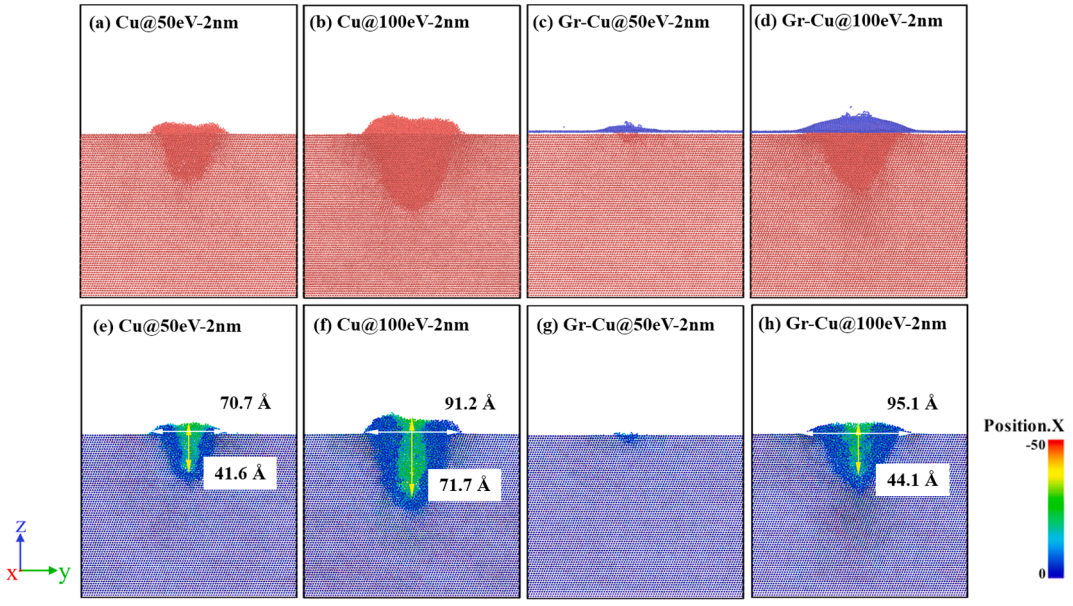

Fig. 9. Erosion crater morphologies of the pure Cu and Gr-Cu systems after the bombardment process with an ion dose of 300 ions with an incident area diameter of 2 nm. In (a)–(d), the red represents Cu atoms, and the blue represents C atoms. (e)–(h) are the cross sections of pure Cu and Gr-Cu systems. The graphene layer is not displayed in (g) and (h). The colour represents the positions of atoms along x-axis, referring to Fig. 7(a_1). (For interpretation of the references to colour in this figure legend, the reader is referred to the web version of this article.)

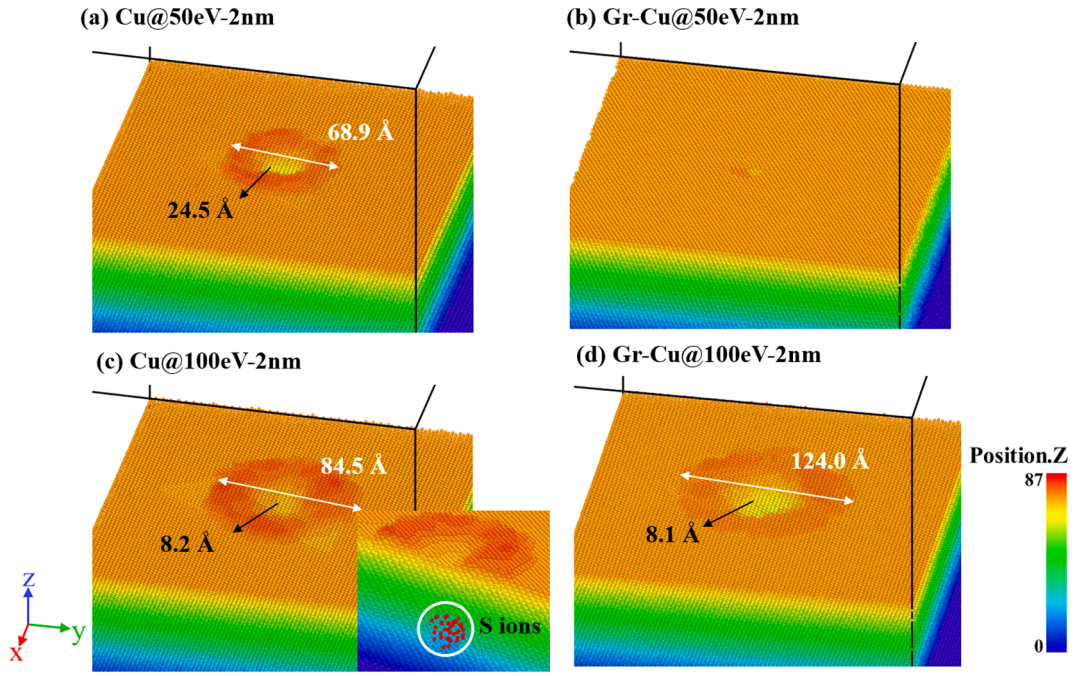

Fig. 10. Surface morphology of pure Cu and Gr-Cu systems cooled down to 300 K after the ion bombardment process with 300 ion dose and an incident area diameter of 2 nm. Graphene layer is not displayed in (b) and (d). Colour represents the position of atoms along the z-axis. Width of the residual erosion crater is marked in white and the depth is marked in black. (For interpretation of the references to colour in this figure legend, the reader is referred to the web version of this article.)

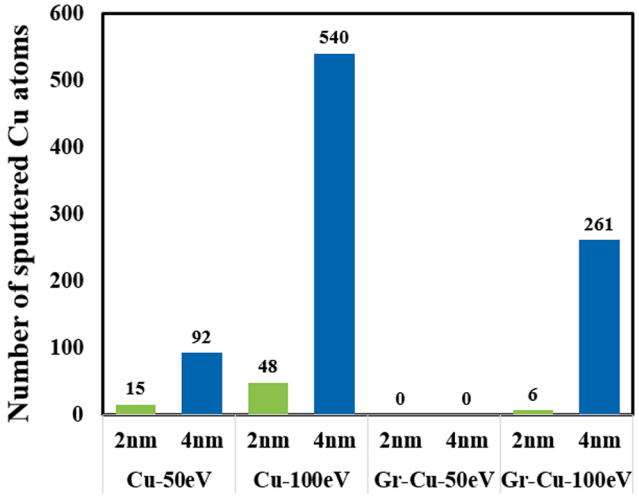

Fig. 11. Impact of the incident area diameter on the number of sputtered Cu atoms.

to the simulation results at 50 eV, doubling the size of the incident area diameter will result in a nearly six times increase in the number of sputtering atoms. Therefore, the size of the arc root could be one of the main effects of the mass loss of the contact materials.

Results in Section 4.2 showed that when the incident area diameter is 2 nm, nearly 200 ions with 50 eV incident energy can break C—C bonds to form nanopores in graphene. However, when the incident area increases, there is a reduction in the energy applied per unit area on the graphene, which hinders the creation of nanopores in graphene and prevents the sputtering of Cu atoms as in Fig. 11. However, when the incident energy is 100 eV, a single sulphur ion can break the C—C bond. Hence, as the incident area increases, incident ions easily remove the C atoms in the incident area resulting in a larger area of Cu being exposed to the ion bombardment. As a result, the interception effect of graphene on Cu atoms decreases, resulting in more sputtered Cu atoms.

Fig. 13 shows the surface morphology of models with an incident area diameter of 4 nm when the system is cooled to 300 K. The residual erosion crater in the pure Cu system with an incident area diameter of 4 nm is larger and deeper than that obtained for a 2 nm incident area diameter which is shown in Fig. 10. When the diameter of the incident area is 4 nm, the crater generated during the bombardment is wider and larger in volume than the crater generated with an incident area diameter of 2 nm (compare the cross sections of erosion craters in Figs. 9 and 12). Hence, the recovery process for ion bombardment with a 4 nm incident area diameter is slower compared to that of 2 nm diameter, causing the former to have a deeper residual pit.

In the Gr-Cu system, there is no crater on the Cu surface when the incident energy is below 50 eV, which is due to the protection of graphene. With the increase of the incident energy to 100 eV, the residual erosion crater in the Gr-Cu system with an incident area diameter of 4 nm becomes larger and deeper than that obtained for the incident area diameter of 2 nm. However, it is shallower and has less bulging of Cu than that in the pure Cu system. Therefore, graphene covered on Cu surface can effectively reduce the damages caused by ions bombardment.

5. Conclusion

The impact of graphene reinforcement on Cu-W MMCs arc erosion resistance was studied through molecular dynamics simulation. Due to the complexity of arc generation and arc erosion process, only the impact of ion bombardment was studied as one of the key erosion processes. Two models built with pure Cu and Cu covered with a graphene layer were bombarded by sulphur ions with different incident energy values, ion dose values and incident area diameter values. Arc erosion resistance was evaluated through multiple parameters, including the sputtering yield, maximum number of vacancies and surface morphology.

Under the same ion bombardment conditions, Cu with the graphene layer had fewer vacancies and sputtered atoms than those in the pure Cu

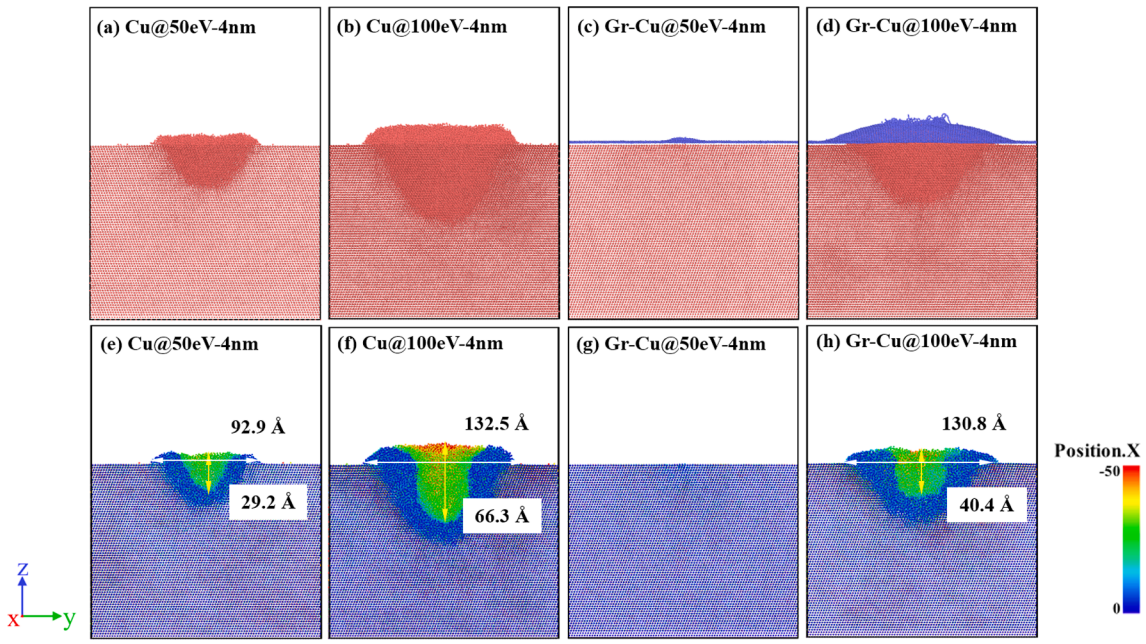

Fig. 12. Erosion crater morphologies of the pure Cu and Gr-Cu systems after the bombardment process with an ion dose of 300 ions with an incident area diameter of 4 nm. In (a)–(d), the red represents Cu atoms, and the blue represents C atoms. (e)–(h) are the cross sections of pure Cu and Gr-Cu systems. The graphene layer is not displayed in (g) and (h). The colour represents the positions of atoms along x-axis, referring to Fig. 7(a_1). (For interpretation of the references to colour in this figure legend, the reader is referred to the web version of this article.)

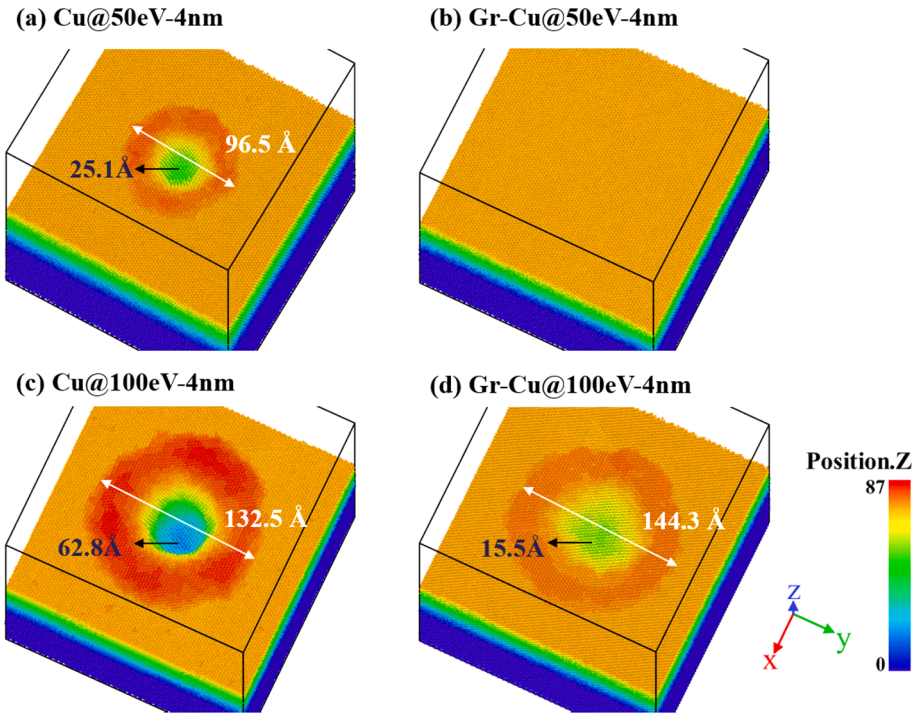

Fig. 13. Surface morphology of pure Cu and Gr-Cu systems cooled down to 300 K after the ion bombardment process with 300 ion dose and an incident area diameter of 4 nm. Graphene layer is not displayed in (b) and (d). Colour represents the positions of atoms along the z-axis. Width of the residual erosion crater is marked in white and the depth in black. (For interpretation of the references to colour in this figure legend, the reader is referred to the web version of this article.)

system. The difference was significantly high when the incident energy of sulphur ions was less than the energy threshold for a sulphur ion to penetrate the graphene layer (~85 eV). In general, the sputtering yield in both models gradually decreased with the increase in ion dose and maintained at a very low value thereafter. This is due to the difficulty in removing Cu atoms from deep positions of the crater as the atoms splashed from the bottom of the well tend to attach to the wall of the molten erosion crater.

The reduction in the number of sputtered atoms and the number of vacancies in the Cu-Gr model can be explained through two phenomena. The first is the ability of graphene to dissipate some of the energy transferred from incident ions as a shock wave, resulting in a reduction

in the energy acting on Cu. The second is the excellent mechanical properties and the high melting point of graphene, which prevents the penetration of recoiled Cu atoms through the graphene layer. Hence the sputtered Cu atoms have to pass through the nanopores in the graphene, which are caused by incident ions. In addition to the reduction in the number of sputtered atoms, these phenomena also result in less bulging in the Cu surface and shallower erosion craters in the Gr-Cu system than in the pure Cu system.

The number of sputtered Cu atoms in the pure Cu system increased drastically with the increase in the diameter of the incident area, which is due to the increase in the surface area exposed to the bombardment. This results in craters that are wider in diameter but shallower compared to those occurred from smaller incident area diameters. Furthermore, these craters have a slower recovery process than the narrow and deeper craters, resulting in deeper residual pits after the cooling process. The impact of the incident area diameter was negligible on the Gr-Cu system when the incident energy was less than the energy threshold of penetrating the graphene layer. However, at high energy levels, the graphene layer exposed to the incident area is completely destroyed, exposing Cu in that area to the ion bombardment process resulting in a large number of sputtered Cu atoms and vacancies.

Overall the simulation results demonstrated the sputtering of materials and the formation of erosion craters during arc erosion from an atomic level. Moreover, by comparing the damages to pure Cu and graphene-covered Cu, this work explained how the addition of graphene reduces the mass loss of Cu and the size of residual erosion craters.

CRediT authorship contribution statement

Ruoyu Xu: Funding acquisition, Supervision. **Mingyu Zhou:** Funding acquisition, Supervision. **Xin Wang:** Writing – original draft, Writing – review & editing. **Shanika Yasantha Matharage:** Writing – review & editing. **Jiu Dun Yan:** Writing – review & editing. **Andrew Connolly:** Writing – review & editing. **Yi Luo:** Funding acquisition, Supervision. **Yi Ding:** Funding acquisition, Supervision. **Zhongdong Wang:** Writing – review & editing, Project administration.

Declaration of Competing Interest

The authors declare that they have no known competing financial interests or personal relationships that could have appeared to influence the work reported in this paper.

Acknowledgement

This work was supported by the State Grid Corporation of China science and technology Foundation (5500-201958505A-0-0-00).

References

[1] R.D. Garzon, High Voltage Circuit Breakers: Design and Applications, second ed., CRC Press, New York, 2002, 10.1201/9780203910634.
[2] H. Ito, Switching Equipment, Springer International Publishing, Cham, 2019, 10.1007/978-3-319-72538-3.
[3] I.A. Glebov, F.G. Rootberg, V.S. Borodin, High-power plasma generators, Plasma Devices Oper. 1 (1) (1990) 31–41, https://doi.org/10.1080/10519999008225527.
[4] M.F. Zhukov, Electric arc generators of thermal plasma (review), Plasma Devices Oper. 5 (1) (1996) 1–36, https://doi.org/10.1080/10519999608228824.
[5] B. Bareyt, A 170-kA DC circuit breaker for the quench protection of the central solenoid coil of the ITER tokamak, Fusion Eng. Des. 54 (1) (2001) 49–61, https://doi.org/10.1016/S0920-3796(00)00106-X.
[6] S.M.G. Ali, H.M. Ryan, D. Lightle, D.W. Shimmin, S. Taylor, G.R. Jones, High power short circuit studies on a commercial 420 kV 60 kA puffer circuit breaker, IEEE Trans. Power Appar. Syst. PAS-104 (2) (1985) 458–467, https://doi.org/10.1109/TPAS.1985.319062.
[7] L.L. Dong, M. Ahangarkani, W.G. Chen, Y.S. Zhang, Recent progress in development of tungsten-copper composites: fabrication, modification and applications, Int. J. Refract. Met. Hard Mater. 75 (March) (2018) 30–42, https://doi.org/10.1016/j.ijrmhm.2018.03.014.
[8] C. Hou, X. Song, F. Tang, Y. Li, L. Cao, J. Wang, Z. Nie, W–Cu composites with submicron- and nanostructures: progress and challenges, NPG Asia Mater 11 (1) (2019).
[9] X. Yang, J. Zou, P. Xiao, X. Wang, Effects of Zr addition on properties and vacuum arc characteristics of Cu-W alloy, Vacuum 106 (2014) 16–20, https://doi.org/10.1016/j.vacuum.2014.03.009.
[10] F.T.N. Vüllers, R. Spolenak, From solid solutions to fully phase separated interpenetrating networks in sputter deposited 'immiscible' W-Cu thin films, Acta Mater. 99 (2015) 213–227, https://doi.org/10.1016/j.actamat.2015.07.050.
[11] E. Tejado, A.V. Müller, J.H. You, J.Y. Pastor, The thermo-mechanical behaviour of W-Cu metal matrix composites for fusion heat sink applications: the influence of the Cu content, J. Nucl. Mater. 498 (2018) 468–475, https://doi.org/10.1016/j.jnucmat.2017.08.020.
[12] G.C. Ma, J.L. Fan, H.R. Gong, Mechanical behavior of Cu-W interface systems upon tensile loading from molecular dynamics simulations, Comput. Mater. Sci. 152 (November 2017) (2018) 165–168. doi: 10.1016/j.commatsci.2018.05.030.
[13] W. Cao, S. Liang, Z. Gao, X. Wang, X. Yang, Effect of Fe on vacuum breakdown properties of CuW alloys, Int. J. Refract. Met. Hard Mater. 29 (6) (Nov. 2011) 656–661, https://doi.org/10.1016/J.IJRMHM.2011.04.014.
[14] C. Leung, E. Streicher, D. Fitzgerald, D. Ilich, Microstructure effect on reignition and welding properties of copper-tungsten electric contact, Electr. Contacts, Proc. Annu. Holm Conf. Electr. Contacts (2003) 132–138, https://doi.org/10.1109/HOLM.2003.1246488.
[15] C. Lee, X. Wei, J.W. Kysar, J. Hone, Measurement of the elastic properties and intrinsic strength of monolayer graphene, Science 321 (5887) (2008) 385–388.
[16] K.S. Novoselov, A.K. Geim, S.V. Morozov, D. Jiang, Y. Zhang, S.V. Dubonos, I. V. Grigorieva, A.A. Firsov, Electric field effect in atomically thin carbon films, Science 306 (5696) (2004) 666–669.
[17] G. Reina, J.M. González-Domínguez, A. Criado, E. Vázquez, A. Bianco, M. Prato, Promises, facts and challenges for graphene in biomedical applications, Chem. Soc. Rev. 46 (15) (2017) 4400–4416, https://doi.org/10.1039/c7cs00363c.
[18] A.A. Balandin, S. Ghosh, W. Bao, I. Calizo, D. Teweldebrhan, F. Miao, C.N. Lau, Superior thermal conductivity of single-layer graphene, Nano Lett. 8 (3) (2008) 902–907.
[19] K. Chu, C. Jia, Enhanced strength in bulk graphene-copper composites, Phys. Status Solidi Appl. Mater. Sci. 211 (1) (2014) 184–190, https://doi.org/10.1002/pssa.201330051.
[20] Y. Fan, Y. Xiang, H.-S. Shen, Temperature-dependent mechanical properties of graphene/cu nanocomposites with in-plane negative Poisson's ratios, Research 2020 (2020) 1–12.
[21] J. Hwang, T. Yoon, S.H. Jin, J. Lee, T.-S. Kim, S.H. Hong, S. Jeon, Enhanced mechanical properties of graphene/copper nanocomposites using a molecular-level mixing process, Adv. Mater. 25 (46) (2013) 6724–6729.
[22] S. Zhang, P. Huang, F. Wang, Graphene-boundary strengthening mechanism in Cu/graphene nanocomposites: a molecular dynamics simulation, Mater. Des. 190 (2020) 108555, https://doi.org/10.1016/j.matdes.2020.108555.
[23] X. Gao, H. Yue, E. Guo, H. Zhang, X. Lin, L. Yao, B. Wang, Mechanical properties and thermal conductivity of graphene reinforced copper matrix composites, Powder Technol. 301 (2016) 601–607.
[24] T. Varol, A. Canakci, Microstructure, electrical conductivity and hardness of multilayer graphene/Copper nanocomposites synthesized by flake powder metallurgy, Met. Mater. Int. 21 (4) (2015) 704–712, https://doi.org/10.1007/s12540-015-5058-6.
[25] M.u. Cao, D.-B. Xiong, Z. Tan, G. Ji, B. Amin-Ahmadi, Q. Guo, G. Fan, C. Guo, Z. Li, D.i. Zhang, Aligning graphene in bulk copper: Nacre-inspired nanolaminated architecture coupled with in-situ processing for enhanced mechanical properties and high electrical conductivity, Carbon N. Y. 117 (2017) 65–74.
[26] K. Zhou, W.G. Chen, J.J. Wang, G.J. Yan, Y.Q. Fu, W-Cu composites reinforced by copper coated graphene prepared using infiltration sintering and spark plasma sintering: a comparative study, Int. J. Refract. Met. Hard Mater. 82 (March) (2019) 91–99, https://doi.org/10.1016/j.ijrmhm.2019.03.026.
[27] L.u. Wang, J. Jin, P. Yang, S. Li, S. Tang, Y. Zong, Q. Peng, Effect of interfacial bonding on dislocation strengthening in graphene nanosheet reinforced iron composite: a molecular dynamics study, Comput. Mater. Sci. 191 (2021) 110309.
[28] J.-Q. Zhu, X. Liu, Q.-S. Yang, Atomistic simulation of the nanoindentation behavior of graphene/Al multilayered nanocomposites, IOP Conf. Ser.: Mater. Sci. Eng. 531 (1) (2019) 012055.
[29] L.A. Yolshina, R.V. Muradymov, I.V. Korsun, G.A. Yakovlev, S.V. Smirnov, Novel aluminum-graphene and aluminum-graphite metallic composite materials: Synthesis and properties, J. Alloys Compd. 663 (2016) 449–459, https://doi.org/10.1016/j.jallcom.2015.12.084.
[30] J.Q. Zhu, Q.S. Yang, X.Q. He, K.K. Fu, Micro-mechanism of interfacial separation and slippage of graphene/aluminum nanolaminated composites, Nanomaterials 8 (12) (2018). doi: 10.3390/NANO8121046.
[31] L. Dong, W. Chen, N. Deng, J. Song, J. Wang, Investigation on arc erosion behaviors and mechanism of W70Cu30 electrical contact materials adding graphene, J. Alloys Compd. 696 (2017) 923–930, https://doi.org/10.1016/j.jallcom.2016.12.044.
[32] L. Dong, W. Chen, C. Zheng, N. Deng, Microstructure and properties characterization of tungsten–copper composite materials doped with graphene, J. Alloys Compd. 695 (2017) 1637–1646, https://doi.org/10.1016/j.jallcom.2016.10.310.
[33] G.A. Haas, R.E. Thomas, Work function and secondary emission studies of various Cu crystal faces, J. Appl. Phys. 48 (1) (1977) 86–93, https://doi.org/10.1063/1.323329.

[34] C.J. Fall, N. Binggeli, A. Baldereschi, Theoretical maps of work-function anisotropies, Phys. Rev. B - Condens. Matter Mater. Phys. 65 (4) (2002) 1–6, https://doi.org/10.1103/PhysRevB.65.045401.
[35] G. Giovannetti, P.A. Khomyakov, G. Brocks, V.M. Karpan, J. Van Den Brink, P. J. Kelly, Doping graphene with metal contacts, Phys. Rev. Lett. 101 (2) (2008) 4–7, https://doi.org/10.1103/PhysRevLett.101.026803.
[36] S.K. Singh, M. Neek-Amal, F.M. Peeters, Melting of graphene clusters, Phys. Rev. B - Condens. Matter Mater. Phys. 87 (13) (2013) 1–9, https://doi.org/10.1103/PhysRevB.87.134103.
[37] J. Tepper, M. Seeger, T. Votteler, V. Behrens, T. Honig, Investigation on erosion of Cu/W contacts in high-voltage circuit breakers, IEEE Trans. Components Packag. Technol. 29 (3) (2006) 658–665, https://doi.org/10.1109/TCAPT.2006.880476.
[38] P.G. Slade, Opening electrical contacts: the transition from the molten metal bridge to the electric arc, IEICE Trans. Electron. E93.C (9) (2010) 1380–1386.
[39] P. G. Slade, Electrical Contacts: Principles and Applications, second ed. CRC Press, 2014. ISBN: 978-1-4398-8131-6.
[40] M.S. Benilov, Theory and modelling of arc cathodes, Plasma Sources Sci. Technol. 11 (3A) (2002) A49, https://doi.org/10.1088/0963-0252/11/3A/307.
[41] M. H. Kim, K. H. Kim, A. Smajkic, M. Kapetanovic, and M. Muratovic, "Influence of contact erosion on the state of SF6 gas in interrupter chambers of HV SF6 circuit breakers, Proc. 2014 IEEE Int. Power Modul. High Volt. Conf. IPMHVC 2014, pp. 466–469, 2015. doi: 10.1109/IPMHVC.2014.7287312.
[42] M. Rong, Q. Ma, Y. Wu, T. Xu, A.B. Murphy, The influence of electrode erosion on the air arc in a low-voltage circuit breaker, J. Appl. Phys. 106 (2) (2009) 023308, https://doi.org/10.1063/1.3176983.
[43] X. Zhou, J. Heberlein, E. Pfender, Theoretical study of factors influencing arc erosion of cathode, IEEE Trans. Compon. Packag. Manuf. Technol. Part A 17 (1) (1994) 107–112, https://doi.org/10.1109/95.296375.
[44] J.A. Rich, Resistance heating in the arc cathode spot zone, J. Appl. Phys. 32 (6) (1961) 1023–1031.
[45] R.W. Liebermann, J.J. Lowke, Radiation emission coefficients for sulfur hexafluoride arc plasmas, J. Quant. Spectrosc. Radiat. Transf. 16 (3) (Mar. 1976) 253–264, https://doi.org/10.1016/0022-4073(76)90067-4.
[46] F.Y. Chu, SF6 Decomposition in Gas-Insulated Equipment, IEEE Trans. Electr. Insul. EI-21 (5) (1986) 693–725, https://doi.org/10.1109/TEI.1986.348921.
[47] R. Tang, J. Callaway, Electron structure to SF6, J. Chem. Phys. 84 (12) (1986) 6854, https://doi.org/10.1063/1.450850.
[48] S. Plimpton, Fast parallel algorithms for short-range molecular dynamics, J. Comput. Phys. 117 (1) (1995) 1–19, https://doi.org/10.1006/JCPH.1995.1039.
[49] S.J. Stuart, A.B. Tutein, J.A. Harrison, A reactive potential for hydrocarbons with intermolecular interactions, J. Chem. Phys. 112 (14) (2000) 6472, https://doi.org/10.1063/1.481208.
[50] M.J. Demkowicz, R.G. Hoagland, Simulations of collision cascades in Cu-Nb layered composites using an EAM interatomic potential, Int. J. Appl. Mech. 1 (3) (Sep. 2009) 421–442, https://doi.org/10.1142/S1758825109000216.
[51] H. Huang, X. Tang, F. Chen, J. Liu, D. Chen, Role of graphene layers on the radiation resistance of copper–graphene nanocomposite: Inhibiting the expansion of thermal spike, J. Nucl. Mater. 493 (2017) 322–329, https://doi.org/10.1016/j.jnucmat.2017.06.023.
[52] S.P. Huang, D.S. Mainardi, P.B. Balbuena, Structure and dynamics of graphite-supported bimetallic nanoclusters, Surf. Sci. 545 (3) (Nov. 2003) 163–179, https://doi.org/10.1016/J.SUSC.2003.08.050.
[53] J.F. Ziegler, J.P. Biersack, The stopping and range of ions in matter, Treatise Heavy-Ion Sci. (1985) 93–129, https://doi.org/10.1007/978-1-4615-8103-1_3.
[54] H. Huang, X. Tang, K. Xie, Q. Peng, Enhanced self-healing of irradiation defects near a Ni–graphene interface by damaged graphene: Insights from atomistic modeling, J. Phys. Chem. Solids 151 (2021) 109909, https://doi.org/10.1016/j.jpcs.2020.109909.
[55] C. Yan, Q.Y. Zhang, Study on low-energy sputtering near the threshold energy by molecular dynamics simulations, AIP Adv. 2 (3) (2012) 32107, https://doi.org/10.1063/1.4738951.
[56] P. Sigmund, Theory of sputtering. I. Sputtering yield of amorphous and polycrystalline targets, Phys. Rev. 184 (2) (1969) 383–416.
[57] P.G. Turchanin, M.A. Agraval, Cohesive energy, properties, and formation energy of transition metal alloys, Powder Metall. Met. Ceram. 47 (2008) 26–39. doi: 10.1007/s11106-008-0006-3.
[58] J.W. Burnett, M.J. Pellin, W.F. Calaway, D.M. Gruen, J.T. Yates, Ion dose dependence of the sputtering yield of Ru(0001) at very low fluences, Phys. Rev. Lett. 63 (5) (1989) 562–565, https://doi.org/10.1103/PHYSREVLETT.63.562.
[59] G. Betz, M.J. Pellin, J.W. Burnett, D.M. Gruen, Low primary ion fluence dependence of single crystal sputtering: a molecular dynamics study, Nucl. Instrum. Meth. Phys. Res. Sect. B: Beam Interact. Mater. Atoms 58 (3–4) (1991) 429–437.
[60] V.S. Smentkowski, Trends in sputtering, Prog. Surf. Sci. 64 (1–2) (May 2000) 1–58, https://doi.org/10.1016/S0079-6816(99)00021-0.
[61] C. Ding, C. Li, C. Fang, Erosion of Cu–W contact material of SF6 circuit breakers when making capacitor bank, IEEJ Trans. Electr. Electron. Eng. 15 (2) (Feb. 2020) 187–193, https://doi.org/10.1002/TEE.23044.